Nano-electromanipulation of Spin Crossover Nanorods: Towards Switchable Nanoelectronic Devices

Aurelian Rotaru, Julien Dugay, Reasmey P. Tan, Il'ya A. Gural'skiy, Lionel Salmon, Philippe Demont, Julian Carrey, Gábor Molnár, Marc Respaud, and Azzedine Bousseksou**

Switching the electronic or magnetic states of molecules or assemblies of molecules is one of the foremost paradigms in molecular electronics. Up to now numerous switchable molecular compounds have been synthesized, involving different physical phenomena, but the common challenge remains the construction of active devices. In particular, devices based on charge transport properties attract a great deal of attention, due to the substantial technological developments accomplished to probe charge transport down to the single molecule level. Here we focus on the charge transport properties of nano-objects displaying molecular spin-state switching. We used electric-field-assisted directed assembly to organize high aspect-ratio spin crossover nanorods between interdigitated electrodes with a very high degree of alignment. The temperature-dependent current-voltage characteristics of each device revealed a bistability of the current intensity associated with the spin-state switching, providing appealing perspectives for nano-scale switching and memory devices.

Spin crossover (SCO) complexes are formed by $3d^4$-$3d^7$ transition metal ions in a quasi-octahedral coordination environment for appropriate values of the ligand field.[1] The switching between the high spin (HS) and low spin (LS) states can be triggered by various external stimuli such as temperature change, light irradiation, the application of pressure or magnetic fields. This spin-state change is accompanied by a spectacular change of various material properties (magnetic, optical, electrical, mechanical, …) providing scope for different applications such as sensors, displays or memories.[2,3] In the last few years, several research groups have focused their attention on the charge transport properties of the SCO compounds, due to their great interest for applications in nanoelectronics and spintronics.[4–15] Recently, we have shown, for the first time, an unambiguous spin-state dependence of the electrical conductivity in powder (both bulk and nanoparticle) samples of the compound $[Fe(Htrz)_2(trz)](BF_4)$ (Htrz = 1H-1,2,4-triazole) by using macroscopic dc conductivity measurements.[9] We have found that the conductivity of this compound increases by (up to) two orders of magnitude when going from the HS to the LS state – due to the lower activation barrier of the conductivity in the latter phase. Our results highlighted also that the spin-state dependence of the electrical conductivity in SCO compounds depends on a subtle interplay between the spin transition temperature and the activation parameters. However, there remains a major challenge in the field which is the integration of SCO nano-objects into real nanoelectronic devices with the main goal to investigate their potential use as switching and memory units as well as to understand their transport properties at the nanometer scale. For these aims it is imperative to control the organization and manipulation of the nano-objects at the device level. In this work, we show a first successful step towards these perspectives through the nano-electromanipulation of SCO nanorods.

To organize the nano-objects between the electrodes we used dielectrophoresis (DEP). This method can be used to manipulate various micro- and nano-sized objects such as nanotubes, nanoparticles, nanowires, biomolecules and can operate in different environments.[16–23] While DEP occurs under both *dc* and *ac* conditions, alternating electric fields are usually employed to suppress undesired electrokinetic and electrochemical phenomena. The DEP force results from the interactions between the non-uniform electric field and the induced dipole moment in a nano-object, and can be attractive or repulsive. A positive (negative) DEP force causes the SCO nano-objects to move towards regions of high (low) field gradient. High aspect ratio objects of a few micrometer size are particularly well suited to dielectrophoretic manipulation. At this size range it is relatively easy to overcome either Brownian motion or gravity by the DEP forces, while the torque felt by non-spherical objects during DEP tends to align their major axis in the direction of the electrical field, leading to well organized assemblies (**Figure 1**).[24–27]

The theory of DEP force and torque are described in details in the Supporting Information (SI). An important parameter for

Dr. A. Rotaru, Dr. I. A. Gural'skiy, Dr. L. Salmon,
Dr. G. Molnár, Dr. A. Bousseksou
Laboratoire de Chimie de Coordination
CNRS UPR-8241 and Université de Toulouse
UPS, INP, F-31077 Toulouse, France
E-mail: gabor.molnar@lcc-toulouse.fr;
azzedine.bousseksou@lcc-toulouse.fr
Dr. A. Rotaru
Faculty of Electrical Engineering and Computer Science
Stefan cel Mare University
13, Str. Universitatii, Suceava 720229, Romania
Dr. J. Dugay, Dr. R. P. Tan, Dr. J. Carrey, Prof. M. Respaud
LPCNO, CNRS UMR-5215 & Université de Toulouse
INSA, UPS, F-31077 Toulouse, France
Dr. I. A. Gural'skiy
Department of Chemistry, National Taras Shevchenko University
01601 Kiev, Ukraine
Prof. P. Demont
LPP-CIRIMAT, CNRS & Université de Toulouse III
31062 Toulouse, France

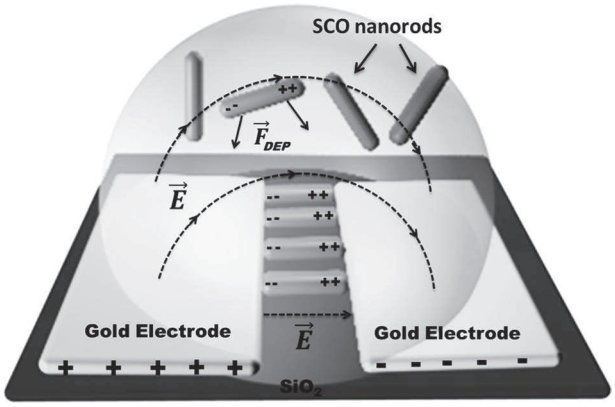

Figure 1. Schematic representation of the device elaboration. The SCO nanorods were organized between the electrodes by diectrophoresis. F_{DEP} represents the dielectrophoretic force acting on a nano-object.

DEP is the ratio of the gap size to the longest axis of the nano-object (denoted by λ). Simulations show that the highest DEP force will be obtained for an optimum value (λ_{max}) in the range of 0.85–1.[25] Indeed, the largest field strengths are located at the edges of the electrodes. As a consequence, for $\lambda < \lambda_{max}$ the electric field felt by the nano-object is weakened. In the same way, when $\lambda > \lambda_{max}$ the DEP force around the nano-object also decreases since the electric field strength is the smallest at the middle of the electrodes. According to the same computational result,[25] the largest torque is obtained when λ is in the range of 0.5–2.0. When λ is larger than 2.0, the torque is decreased by the reduced gradient of the electric field. If λ is smaller than 0.5, the (polarizable) effective length of the nanorods changes from the long to the short axis of the rod, which results in a negligible or negative torque.

In this paper we report studies concerning the nano-scale manipulation and the charge transport properties of high aspect ratio (length/diameter ≈ 12) nano-objects of the $[Fe(Htrz)_2(trz)](BF_4)$ spin crossover compound (**Figure 2**).

Selected scanning electron microscopy (SEM) images of deposits obtained by DEP are shown in Figure 3 (see SI for additional experimental results). These experiments were performed with nanorod suspensions of 0.2 g/L at 7 V_{rms} and 10 kHz using gold electrodes with 4 µm gap, implying $1.05 < \lambda < 1.6$. Owing to these λ values, the torque and DEP force are nearly maximized. One can observe that the nano-objects are strongly forced to move towards the maximum of the external field. They are almost entirely concentrated in the space between the electrodes and the number of nano-objects deposited outside the electrode area is negligible. Another important observation is that the nano-objects are preferentially aligned perpendicular to the electrodes. A manner to quantize this alignment is the orientational order parameter S:

$$S = <2\cos^2\theta - 1> \quad (1)$$

where θ is the angle between a particular nano-object and the mean orientation of all nano-objects, and the brackets denote an average over all observations. Thus $S = 0$ means a random deposit alignment whereas $S = 1$ means perfect order.[26] The statistics shown in the insert of **Figure 3** lead to $S = 0.86$, indicating thus a very high degree of alignment. In these experimental conditions the nanorods form a discontinuous monolayer. However, the quantity of the deposited objects between the electrodes can be easily modified by changing the deposition frequency and/or the concentration of the nanorod suspension. At higher frequencies the coverage tends to decrease (see Figure S1), while – obviously – a higher initial particle concentration leads to higher coverage. For example SEM pictures for a nano-object concentration of $c = 2$ g/L revealed the formation of a very dense multilayer with an orientation order parameter of $S = 0.65$ (see fig. S2). The decreasing alignment of the nanorods with increasing deposit thickness can be explained by a lower value of the electric field for the top layer. Indeed, the electric field simulations shown in **Figure 4** reveal an exponential decrease of the field with increasing distance from the substrate. One shall note also that even if we obtained a good alignment, the average length of the nanorods is slightly smaller than the gap size. Therefore a considerable amount of the nanorods cannot form a single nano-object electrical pathway between the electrodes. To confirm if we can increase the proportion of nanorods directly connecting the electrodes while keeping a high S value, we performed experiments using 2.5 µm electrode gaps ($0.5 < \lambda < 0.8$). With this lower value of λ the torque is not maximized, but we notice that the nanorods are just slightly misaligned ($S = 0.83$) and the number of "single object connections" increases significantly thanks to the smaller electrode gap (see Figures S3 and S4). For comparison, we have also carried out a series of DEP experiments using nanorods

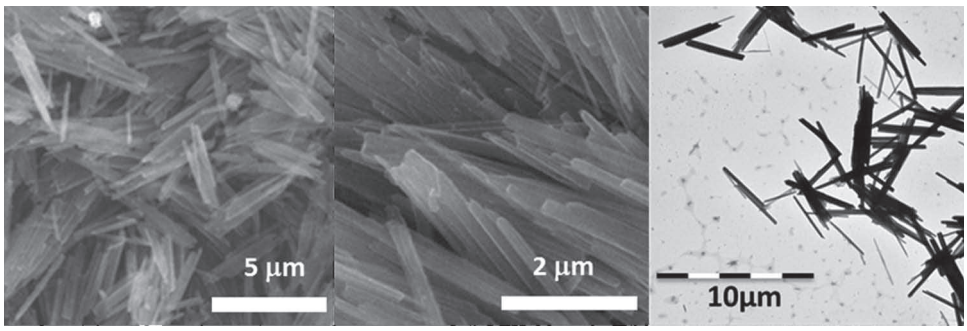

Figure 2. Scanning and transmission electron microscopy images of spin crossover nanorods. The complex $[Fe(Htrz)_2(trz)](BF_4)$ forms rod-like crystallites of 3.1 ± 0.7 µm length and 200–300 nm diameter (aspect ratio ≈ 12).

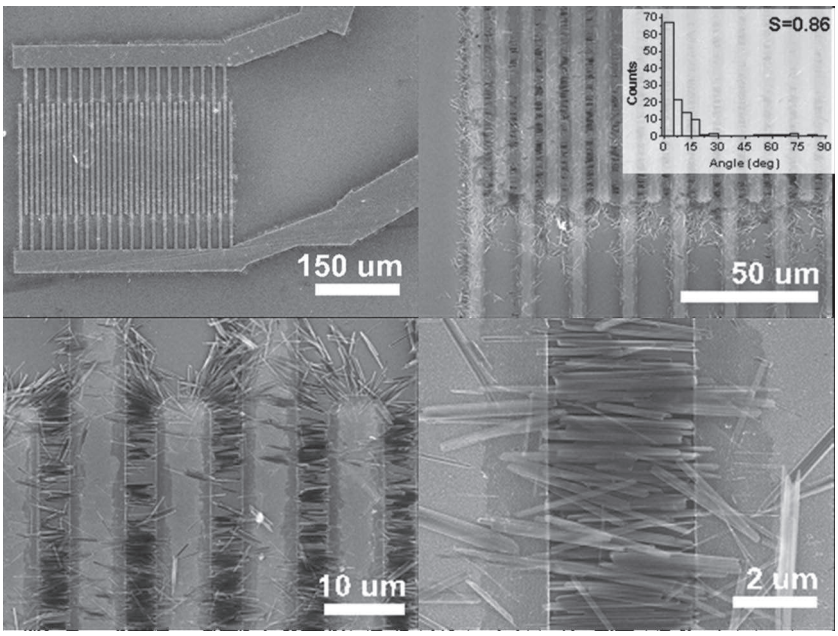

Figure 3. Spin crossover nanorods trapped by dielectrophoresis**.** The SEM images show ordered SCO nanorods deposited within 4 µm electrode gaps. The applied *ac* voltage and frequency were 7 V_{rms} and 10 kHz, respectively, and the nanorod concentration was 0.2 g/L (in ethanol) during the deposition. The insert shows the histogram of the angular distribution of nanorods. The angle value 0° is defined for nanorods parallel to the electric field.

with significantly lower aspect ratio (length: ≈250 nm, diameter: ≈100 nm). These less elongated nano-objects are still attracted between the electrodes despite their smaller size and form a fairly dense monolayer (see Figures S5–S9). However, the long axis of the nano-objects is almost randomly oriented: we observed $S = 0.09$ and $S = 0.16$ for 4 µm and 100 nm electrode gaps, respectively. This observation is a natural consequence of the reduced aspect ratio (≈2.5), which leads to a negligible or negative torque.

The thermal variation of the electrical conductivity, *I(T)*, and current–voltage, *I(V)*, characteristics of the obtained device are reported in **Figure 5**. The *I(V)* curves are non-linear, which arises probably from a voltage activation of the charge transport. The transport can be also thermally activated, as evidenced by the strong temperature dependence of the conductivity. Even more importantly, a hysteresis of *ca.* 40 K width (centred around ca. 370 K) can be depicted in the *I(T)* curve. This hysteresis loop was observed reproducibly, which means that it is not related to sample evolution or degradation, but is a genuine characteristic of the device. Indeed, the observed hysteresis compares well with the data obtained by optical and electrical measurements on the powder sample of the nanorods.[9] This thermal hysteresis is a well-known property of many spin crossover solids and finds its origin in the strong electron-lattice coupling.[1,3] In brief, it is the expansion and deformation of the complex, associated with its spin state change, which gives rise to various cooperative phenomena in these materials, such as the first-order transition in our sample. Although in these measurements the current flow has been recorded through a few nano-objects only, the transport properties are not very different from those previously observed in our group on bulk powder samples with many grain boundaries.[9] These results point out the fact that the charge diffusion at the inter-particle interface is not the major contribution to the overall electrical conductivity. The temperature dependence of the electrical conductivity was also recorded for different device geometries and three different morphology samples and gave similar results in each case, *i.e.* the LS state was found always more conducting (see Figures S9 and S14). One should note here that this spin-state dependence of the electrical conductivity is in disagreement with the results obtained by Prins et al.[8] who reported on a more conducting HS state for similar (though somewhat smaller) nanoparticles. These opposite findings suggest different charge transport mechanisms. Indeed, it is important to underline that in our study we measured the current flow through an electrode gap of (at least) 100 nm, while a 10-nm gap was used in ref.[8] The charge transport mechanism in our case is thought to be dominated therefore by thermally-activated hopping of charge carriers,[9] while the charge transport in the device of Prins et al. was suggested to occur by single electron tunneling.[8] However, a detailed comparison between the two experiments would be extremely speculative at this stage for the lack of details about the transport mechanisms and also due to the fact that these mechanisms can be rather sensitive to various experimental details (sample morphology, contacts, impurities, …).

In summary, we successfully applied dielectrophoresis to trap and organize spin crossover nano-objects between interdigitated electrodes with particularly good results in the case of high aspect-ratio nanorods. We succeeded in recording the

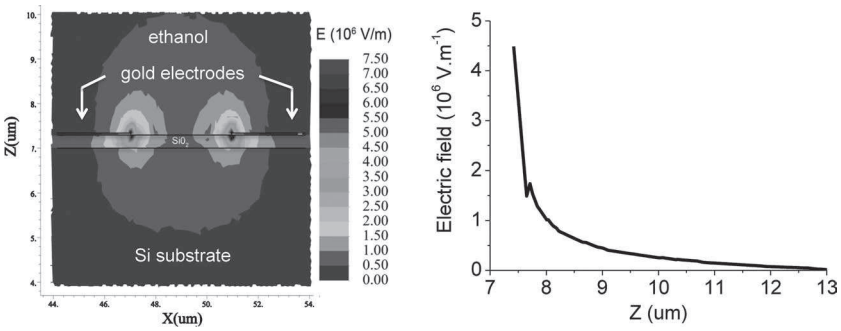

Figure 4. Simulation of the electric field during dielectrophoresis (corresponding to the experiment in Figure 3). The "finger-like" electrodes are spaced 4 µm apart. The applied potential is 7 V_{rms}. The relative permittivities used for simulations are 5, 11.8, 22.4 and 1000 for the oxide layer, the Si substrate, ethanol and gold electrodes, respectively.

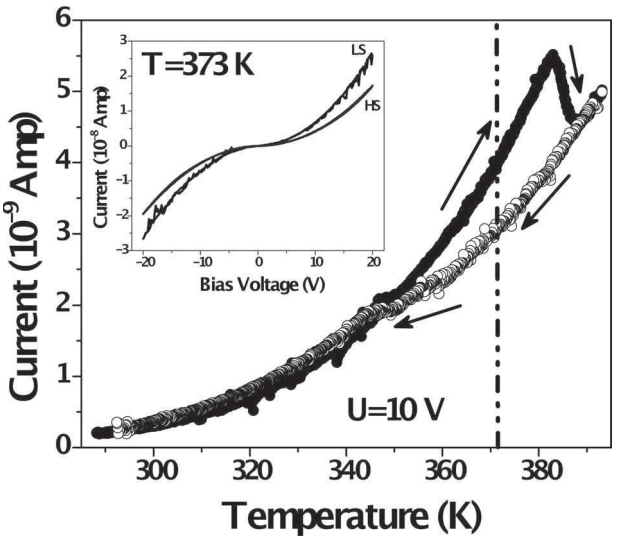

Figure 5. Device electrical characterization. Current intensity recorded under a bias voltage of 10 V as a function of temperature in the heating and cooling modes. The inset shows the current–voltage characteristics recorded within the thermal hysteresis region at 373 K in the heating (low spin) and cooling (high spin) modes.

thermal spin state dependence of the device electrical characteristics for different morphology nano-objects and for different device geometries. In agreement with previous measurements on powder samples, for each device we observed a thermal hysteresis of the current intensity, with systematically higher currents when the particles were switched from the HS to the LS state. These results reveal that one-dimensional spin crossover nanostructures are very attractive building blocks for nanoelectronic switching and memory devices and open also the way towards the study of the size effect in single SCO objects. This paper should therefore strongly encourage chemists to develop methods for the growth of such bistable nanorods and nanowires, which are not readily available today.[3]

Experimental Section

Details of the synthesis and characterization of the nano-objects are given in ref. [9] and in the Supporting Information. Here we shall stress only that no surfactants were used, which could alter the electrical properties of the device. It may be worth to note also that the elongated shape of the nanorods is almost certainly a consequence of the specific structure of this family of iron(II)-triazole complexes, forming "infinite" $[Fe(Rtrz)_3]_n$ chains.[28]

Standard photolithography and electron-beam lithographywere used to make three sets of interdigitated gold electrodes (5 nm Ti, 30 nm Au) on a silicon substrate with a 300 nm silicon oxide layer. The choice of such interdigitated electrodes has been motivated by the wish to enhance the electrical current intensity for transport measurements. Electrodes with gaps of 100 nm, 2.5 μm and 4 μm have been fabricated. For the elaboration of the final device, a colloidal suspension of the nano-objects is required. For this purpose, the nanorods have been dispersed in ethanol and ultrasonicated for about 10 seconds to disperse the aggregates. For each experiment a 13 μL droplet of the nano-object suspension was deposited on the substrate by manual pipetting. Then the electrodes were connected to an *ac* voltage source for approximately 15 s and, afterwards, the excess of nano-object suspension was removed. In the applied *ac* frequency range (1–100 kHz), no electro-osmotic flow is generated due to ion movement (see SI for more details). According to the DEP formula (see SI), for higher field strengths the DEP force is higher and there is also a better alignment by the torque. Therefore, in our experiments we applied the maximum accessible *ac* voltage (7 V_{rms}).

SEM images were recorded using a Hitachi S4800 microscope operating at 15 kV. Electrical characterization of the devices has been carried out under bias voltages up to 10 V using a Keithley source-meter (model 6430), connected to a micro-manipulated probe station, which was equipped with two *dc* probes. The temperature was changed at a rate of 3 K/min in the heating and cooling modes by means of a Linkam PE120 variable temperature stage. Numerical simulations of the electric field distribution were carried out using commercially available software (FlexPDE[29]).

Acknowledgements

Financial support from the projects CrossNanomat (ANR) and TRAIN^2 (SUDOE) is acknowledged. The work at Suceava was supported by a grant of the Romanian National Authority for Scientific Research, CNCS–UEFISCDI, project number PN-II-RU-TE-2011-3-0307. Technical support from ITAV (Bionanotechnology platform) is also acknowledged.

[1] *Spin-Crossover in Transition Metal Compounds* (Ed: P. Gütlich, H. Goodwin), *Topics in Current Chemistry*, Vols. *233–325*, Springer-Verlag, Berlin, **2004**.
[2] O. Kahn, C. J. Martinez, *Science* **1998**, *279*, 44.
[3] A. Bousseksou, G. Molnar, L. Salmon, W. Nicolazzi, *Chem. Soc. Rev.* **2011**, *40*, 3313.
[4] L. Salmon, G. Molnar, S. Cobo, P. Oulie, M. Etienne, T. Mahfoud, P. Demont, A. Eguchi, H. Watanabe, K. Tanakae, A. Bousseksou, *New J. Chem.* **2009**, *33*, 1283–1289.
[5] T. Mahfoud, G. Molnar, S. Cobo, L. Salmon, C. Thibault, C. Vieu, P. Demont, A. Bousseksou, *Appl. Phys. Lett.* **2011**, *99*, 053307.
[6] M. S. Alam, M. Stocker, K. Gieb, P. Muller, M. Haryono, K. Student, A. Grohmann, *Angew. Chem, Int. Ed.* **2010**, *49*, 1159.
[7] V. Meded, A. Bagrets, K. Fink, R. Chandrasekar, M. Ruben, F. Evers, A. Bernand-Mantel, J. S. Seldenthuis, A. Beukman, H. S. J. van der Zant, *Phys. Rev. B* **2011**, *83*, 245415.
[8] F. Prins, M. Monrabal-Capilla, E. A. Osorio, E. Coronado, H. S. J. van der Zant, *Adv. Mater.* **2011**, *23*, 1545.
[9] A. Rotaru, I. A. Gural'skiy, G. Molnár, L. Salmon, P. Demont, A. Bousseksou, *Chem. Commun.* **2012**, *48*, 4163–4165.
[10] C. Etrillard, V. Faramarzi, J.-F. Dayen, J.-F. Létard, B. Doudin, *Chem. Commun.* **2011**, *47*, 9663.
[11] D. Aravena, E. Ruiz, *J. Am. Chem. Soc.* **2011**, *134*, 777.
[12] S. Shi, G. Schmerber, J. Arabski, J. B. Beaufrand, D. J. Kim, S. Boukari, M. Bowen, N. T. Kemp, N. Viart, G. Rogez, E. Beaurepaire, H. Aubriet, J. Petersen, C. Becker, D. Ruch, *Appl. Phys. Lett.* **2009**, *95*, 043303.
[13] C. Faulmann, K. Jacob, S. Dorbes, S. Lampert, I. Malfant, M. L. Doublet, L. Valade, J. A. Real, *Inorg. Chem.* **2007**, *46*, 8548.

[14] K. Takahashi, H. B. Cui, Y. Okano, H. Kobayashi, Y. Einaga, O. Sato, *Inorg. Chem.* **2006**, *45*, 5739.
[15] M. Nihei, N. Takahashi, H. Nishikawa, H. Oshio, *Dalton Trans.* **2011**, *40*, 2154.
[16] A. Vijayaraghavan, S. Blatt, D. Weissenberger, M. Oron-Carl, F. Hennrich, D. Gerthsen, H. Hahn, R. Krupke, *Nano Lett.* **2007**, *7*, 1556–1560.
[17] R. Krupke, F. Hennrich, H. B. Weber, M. M. Kappes, H. von Lohneysen, *Nano Lett.* **2003**, *3*, 1019–1023.
[18] J. Dugay, R. P. Tan, A. Meffre, T. Blon, L.-M. Lacroix, J. Carrey, P. F. Fazzini, S. Lachaize, B. Chaudret, M. Respaud, *Nano Lett.* **2011**, *11*, 5128.
[19] K. A. Brown, R. M. Westervelt, *Nano Lett.* **2011**, *11*, 3197.
[20] J. J. Boote, S. D. Evans, *Nanotechnology* **2005**, *16*, 1500–1505.
[21] R. W. Clarke, S. S. White, D. J. Zhou, L. M. Ying, D. Klenerman, *Angew. Chem. Int. Ed.* **2005**, *44*, 3747–3750.
[22] S. B. Asokan, L. Jawerth, R. L. Carroll, R. E. Cheney, S. Washburn, R. Superfine, *Nano Lett.* **2003**, *3*, 431–437.
[23] C. H. Lee, D. R. Kim, X. Zheng, *Nano Lett.* **2010**, *10*, 5116–5122.
[24] D. E. Chang, N. Petit, *Int. J. Robust Nonlinear Control* **2005**, *15*, 769–784.
[25] Y. Liu, J.-H. Chung, W. K. Liu, R. S. Ruoff, *J. Phys. Chem. B* **2006**, *110*, 14098–14106.
[26] W. Ahmed, E. S. Kooij, A. van Silfhout, B. Poelsema, *Nano Lett.* **2009**, *9*, 3786–3794.
[27] E. M. Freer, O. Grachev, X. Duan, S. Martin, D. P. Stumboscholar, *Nat. Nanotechnol.* **2010**, *5*, 525–530.
[28] A. Grosjean, N. Daro, B. Kauffmann, A. Kaiba, J.-F. Letard, P. Guionneau, *Chem. Commun.* **2011**, *47*, 12382–12384.
[29] PDE Solutions website, http://www.pdesolutions.com (last accessed January 2013).